https://doi.org/10.5194/egusphere-2025-6339
Preprint. Discussion started: 27 January 2026
© Author(s) 2026. CC BY 4.0 License.

Limited atmospheric iron availability increase during the Pleistocene-Holocene transition in the Northern Hemisphere

François Burgay[1,2], Haley Derrod[2], Tobias Erhardt[3,4], Federico Scoto[2,5], Delia Segato[6,2], Niccolò Maffezzoli[2,5,7], Federico Dallo[5], Daniele Zannoni[2], Azzurra Spagnesi[2], Helle-Astrid Kjær[8], Hubertus Fischer[3], Cristiano Varin[2], Carlo Barbante[2,3], Andrea Spolaor[2,3,*]

[1] Department of Environmental Sciences, University of Basel, Basel, Switzerland

[2] Department of Environmental Sciences, Informatics and Statistics, Ca' Foscari University of Venice, Venice Mestre, Italy

[3] Climate and Environmental Physics, Physics Institute & Oeschger Centre for Climate Change Research, University of Bern, Bern, Switzerland

[4] Institute of Geosciences, Goethe University Frankfurt, Frankfurt am Main, Germany

[5] Institute of Polar Sciences, National Research Council, Venice Mestre, Italy

[6] European Commission, Joint Research Centre, Ispra, Italy

[7] Department of Earth System Science, University of California, Irvine, Irvine, United States of America

[8] Physics for Ice, Climate and Earth, Niels Bohr Institute, University of Copenhagen, Copenhagen, Denmark

*Corresponding author: andrea.spolaor@unive.it

KEY POINTS

- Continuous analysis of dissolved iron during the Pleistocene-Holocene transition
- Limited increase in dissolved iron during the Younger Dryas (+29%) compared to the Early Holocene
- Atmospheric iron solubility in the Northern Hemisphere is driven by aerosol acidity changes

https://doi.org/10.5194/egusphere-2025-6339
Preprint. Discussion started: 27 January 2026
© Author(s) 2026. CC BY 4.0 License.

Abstract

Iron (Fe) availability modulates phytoplankton blooms in High-Nutrient Low-Chlorophyll (HNLC) regions, i.e., ocean areas characterized by an abundance of major nutrients but low marine productivity. Fe can be delivered to the oceans through atmospheric dust deposition, making ice cores unique archives for reconstructing past changes in aeolian Fe deposition. However, while it is known that during dustier periods atmospheric Fe depositions increased, uncertainties remain regarding the fraction of Fe actually available to phytoplankton. Here, we present evidence from the EGRIP ice core (Greenland), which allows insights into atmospheric aerosol deposition over the Fe-limited North Pacific Ocean, during the Pleistocene-Holocene transition (10.3-13.0 ka). Results show that, in contrast to the 17-fold enhancement in total Fe concentration, dissolved Fe increased only modestly (+29%) during the Younger Dryas compared to the Early Holocene, likely due to prevailing alkaline aerosol conditions reducing its solubility. This finding supports the hypothesis that factors other than atmospheric Fe deposition (e.g., stronger water stratification, sea-ice extent, volcanic eruptions, iron remobilization from sediments), play a more relevant role in regulating marine net primary productivity in the HNLC North Pacific Ocean over the last glacial transition.

https://doi.org/10.5194/egusphere-2025-6339
Preprint. Discussion started: 27 January 2026
© Author(s) 2026. CC BY 4.0 License.

1. Introduction

Iron (Fe) plays a crucial role in oceanic biogeochemistry, serving as a co-factor in enzymes involved in photosynthesis and atmospheric nitrogen fixation (Mills et al., 2004). Its bioavailability and abundance in the ocean can limit net primary productivity (NPP), even when other major nutrients such as nitrate and phosphate are abundantly present. Regions where this occurs are known as High-Nutrient Low-Chlorophyll (HNLC) areas, which account for up to 20% of the world's ocean surface and include the Southern Ocean, the Equatorial Pacific, and the North Pacific Ocean (Duggen et al., 2010). In these regions, aeolian Fe deposition can act as a fertilizer, triggering and modulating NPP and thus influencing CO_2 exchanges between the atmosphere and the ocean (Martin and Fitzwater, 1988).

The link between iron fertilization and the biological carbon pump was first explored by oceanographer John Martin. His hypothesis, known as the *iron hypothesis*, suggests that higher aeolian iron fluxes deposited on HNLC ocean surfaces during colder and dustier periods would have stimulated NPP, enhancing the drawdown of atmospheric CO_2 into the oceans and explaining the 80-100 ppm lower CO_2 concentrations observed during glacial periods compared to warmer, less dusty, interglacial periods (Martin et al., 1990). Modelling and observational evidence confirmed that Martin's intuition was correct, although the impact of Fe fertilization has since been substantially downscaled (Stoll, 2020). Other processes, such as stronger oceanic stratification during glacial times, played a more important role (Francois et al., 1997; Lambert et al., 2021). Nevertheless, millennial-scale Earth System Model simulations estimated that up to 20 ppm of the glacial CO_2 decline can be still attributed to a more globally efficient biological carbon pump enhanced by atmospheric iron deposition during the last glacial maximum (Lambert et al., 2015).

The response of HNLC regions to Fe fertilization during glacial periods varied regionally. In the Southern Ocean, enhanced atmospheric Fe fluxes induced an increase in NPP in the Subantarctic Zone, as inferred from sea-sediment records (Martínez-García et al., 2014; Jaccard et al., 2013), while the net effect over the whole Southern Ocean was much smaller (Fischer et al., 2025). In the North Pacific Ocean, NPP showed no significant response to enhanced atmospheric Fe fluxes over the last 800 ka

https://doi.org/10.5194/egusphere-2025-6339
Preprint. Discussion started: 27 January 2026
© Author(s) 2026. CC BY 4.0 License.

(Kienast et al., 2004; Burgay et al., 2021a). While limited nutrient upwelling, sea-ice extent and iron remobilization from sediments have been acknowledged as key drivers regulating NPP in this region (Kienast et al., 2004; Praetorius et al., 2015), a crucial question remains unanswered: to what extent was atmospheric aerosol iron actually available to phytoplankton?

Ice cores can address this question by providing highly-temporal resolved information on how iron concentrations changed during past climatic transitions. To quantify iron in ice cores, different methodologies exist, each of them targeting a specific operationally defined Fe fraction. Total dissolved iron (TDFe) is defined as iron determined in discrete samples by Inductively Coupled Plasma Mass Spectrometry (ICP-MS) after at least four weeks of acid (2% HNO_3) digestion at pH = 1 (Burgay et al., 2021a; Edwards and Sedwick, 2001). However, TDFe overestimates the bioavailable Fe fraction as long acidic digestions allow for more complete dissolution of acid-labile Fe (Vallelonga et al., 2013; Edwards et al., 2006). ICP-MS has been also used to continuously quantify Fe after shorter (few seconds) acidification times (Fe_{ICP}). Fe_{ICP} may overestimate the dissolved fraction when a non-negligible amount of undissolved mineral particles is present, such as during dusty periods (Erhardt et al., 2019). The form more readily accessible to phytoplankton (dissolved Fe, DFe) can be quantified using discrete and continuous sampling approaches. Discrete methods typically involve filtering melted ice samples through 0.2 µm or 0.45 µm filters, followed, sometimes, by acidification with HNO_3 (Du et al., 2019). Representative seawater soluble Fe analyses have also been performed by sublimating ice under vacuum, then leaching the residual dust particles with seawater (Conway et al., 2015). Continuous DFe measurements involve online acidification of the meltwater stream from a Continuous Flow Analysis (CFA) system, followed by absorption detection (Burgay et al., 2019; Hiscock et al., 2013). The mild acidification step at pH≈1.6 with HCl releases iron bound from both colloidal forms and iron-binding ligands (Lohan et al., 2006), as well as it breaks down Fe-hydroxides and Fe-complexes into dissolved free Fe (Hiscock et al., 2013). For these reasons, continuous DFe represents the easily leachable, labile fraction, i.e., the form of iron that would be most readily available for complexation by phytoplankton siderophores once deposited in seawater (Yoshida et al., 2002). Therefore, in this work we define continuously measured DFe as the biological active fraction (Hiscock et al., 2013).

https://doi.org/10.5194/egusphere-2025-6339
Preprint. Discussion started: 27 January 2026
© Author(s) 2026. CC BY 4.0 License.

However, dedicated studies assessing the actual bioavailability of DFe quantified by CFA have not yet been performed.

Here, we present the first continuous Fe_{ICP} and DFe measurements during the Pleistocene-Holocene transition (10.3-13.0 ka) from the EGRIP ice core (Greenland), to investigate changes in DFe during the Younger Dryas (YD), a high-dust climate cold event, and the subsequent Preboreal transition into the warm, low-dust Holocene.

2. Material and methods

2.1 EGRIP ice core

The East Greenland Ice-core Project (EGRIP) retrieved a 2665-meter-long ice core to investigate how ice streams may contribute to future sea-level change. The EGRIP drill camp was located within the North-East Greenland Ice Stream (NEGIS), approximately 360 km NNE from the Greenland Summit (Figure S1, 2708 m. a.s.l., 75.63°N, 36.00° W) (Erhardt et al., 2023). The NEGIS drains ice from the interior of the ice sheet towards marine-terminating outlet glaciers in North-East Greenland, at modern surface velocities of 55 m a^{-1} (Hvidberg et al., 2020). The EGRIP ice was therefore likely deposited ≈180 km upstream towards the ice divide at the time of deposition (10.3-13.0 ka), as compared to present day (Gerber et al., 2021). The core was dated using published chronology (GICC05 transfer from NGRIP on volcanic matching), with a maximum counting error (MCE) between 89 (10.3 ka) and 141 (13.0 ka) years (Mojtabavi et al., 2019).

2.2 The Bern Continuous Flow Analysis system (Bern-CFA)

The Bern Continuous Flow Analysis (Bern-CFA) is used to analyze elements and major ions in polar ice cores at a high temporal resolution (≈1 cm-depth resolution). Ice samples were cut with a section of 36x36x550 mm, known as a "bag". The ice is melted at a speed of 2.8 cm min^{-1} along the core axis on a gold-plated melthead inside a -20°C cold room. To remove contamination of the ice due to handling or drilling fluid, only the meltwater from the innermost 26x26 mm of the ice is used for analysis. The resulting meltwater is directed toward two sections for analyses: a *wet-chemistry* and a single particle ICP-TOF-MS (spICP-MS) section. The wet-chemistry line detects soluble Ca^{2+}, NH_4^+,

https://doi.org/10.5194/egusphere-2025-6339
Preprint. Discussion started: 27 January 2026
© Author(s) 2026. CC BY 4.0 License.

NO_3^-, concentration and size distribution of insoluble particles, conductivity, black carbon, acidity, and DFe (Kaufmann et al., 2008; Burgay et al., 2019; Erhardt et al., 2023; Kjær et al., 2016). The spICP-MS line provides continuous trace element profiles and allows single particle characterization in selected intervals (Erhardt et al., 2019). Here, we present a continuous quantification of Fe_{ICP}, acidity, dust and conductivity between 10.3 and 13.0 ka. Eight selected periods during the Holocene (n = 23 bags), Younger Dryas (YD, n = 30) and Bølling-Allerød (BA, n = 16) have been analyzed also for DFe (Table 1).

2.2.1 DFe and Fe_{ICP} continuous quantification

DFe concentrations are quantified using the continuous absorption method described in Burgay et al. (2019) at a resolution of 1 cm. The ice-core meltwater flow for DFe analysis was 0.9 mL min^{-1}. Raw DFe transmittance values (λ = 514 nm) were acquired every second using the OceanView software (Ocean Optics), and later converted into absorption values. Absorbance values were converted into concentration units (µg L^{-1}) using the Beer-Lambert law, with an optical path length set to 1 cm (Figure S2). Calibration curves were performed before and after each analytical run, to account for any sensitivity changes. Calibration standards were prepared by diluting a certified Fe stock solution at 1000 mg L^{-1} ($Fe(NO_3)_3$, Certipur®, Merck) to 0.5-10 µg L^{-1}, based on expected concentrations throughout the record (Table S1). To monitor and correct for blank drifts, ultrapure water samples were analyzed at the beginning and end of each sample run. The DFe limit of detection (LoD), calculated as three times the standard deviation of 10 Ultrapure Water (UPW) blanks, was determined to be 0.08 µg L^{-1}. In correspondence with two specific volcanic eruptions (12.91 and 13.03 ka BP), the spectrophotometric detector saturated, preventing a reliable quantification of DFe for these volcanic horizons.

Fe_{ICP} was quantified using spICP-MS equipped with a collision cell (Q-Cell) that removes isobaric interferences (e.g., $^{40}Ar^{16}O^+$), enabling the determination of the most abundant Fe isotope (^{56}Fe), and a time-of-flight mass spectrometer. Meltwater flow rate was 1.0 mL min^{-1}. The LoD, calculated as three times the standard error of intercept from the calibration curve, was quantified to be 0.12 µg L^{-1}. Resolution is 1 cm. Regular calibrations were performed after each run by diluting certified Fe standard

https://doi.org/10.5194/egusphere-2025-6339
Preprint. Discussion started: 27 January 2026
© Author(s) 2026. CC BY 4.0 License.

solution at 1000 mg L^{-1} (Ventures IV-STOCK-1643 Multielemental standard) to 0.2-1000 µg L^{-1}, based on the expected concentrations throughout the record. Further details in Erhardt et al., (2019).

2.2.2 Acidity, conductivity and dust measurements

Acidity was determined using a continuous absorption method (Kjær et al., 2016) based on two dyes (bromophenol blue and chlorophenol red), which change color, and thus absorption values, depending on pH. Bromophenol blue changes from yellow at pH 3.0 to purple at pH 4.6, while chlorophenol red shifts from yellow at pH 4.8 to violet at pH 6.7. Standard solutions were prepared by diluting 1.0 M HCl and 1.0 NaOH stock solutions. For the Holocene period, standards were prepared at -2.5, 2.5 and 4.9 µeq L^{-1}. For the YD and BA, standards were prepared at -4.9, -2.5 and 2.5 µeq L^{-1}. Calibration curves were performed before and after each analytical run, to account for any sensitivity change. Acidity values should be interpreted qualitatively, as the calibration standards are influenced by CO_2 dissolution from laboratory air, whereas the CFA meltwater stream is likely not. For the purpose of this work, negative values represent standards/samples that are more alkaline than pH = 5.4 (UPW).

In addition to acidity, electrolytic meltwater conductivity was measured using a conductivity cell (3082 with micro flow cell 829, Amber Science), while a laser attenuation particle counter and sizer (Abakus with LDS 23/25bs sensor, Klotz) was used for determining insoluble particle concentrations (Kaufmann et al., 2008; Erhardt et al., 2023; Simonsen et al., 2018).

2.2.3 Raw data treatment and data alignment with the CFA data

Once calibrated, DFe data was aligned with conductivity data provided by the Bern-CFA (SM - Section 1) as previous studies have shown a correlation between these parameters in Holocene samples (Burgay et al., 2019). Cross-correlation techniques were applied as they are commonly used to compare time series and identify the degree of linear similarity between datasets at varying time lags. To measure the time delays between two time series of irregularly sampled data and align them, the Interpolated Cross-Correlation Function (ICCF) was employed (Gaskell and Sparke, 1986). For each sample run, the ICCF was calculated at a sequence of time lags, and the lag corresponding to the maximum correlation value was selected as the optimal alignment point. This process was repeated across the

https://doi.org/10.5194/egusphere-2025-6339
Preprint. Discussion started: 27 January 2026
© Author(s) 2026. CC BY 4.0 License.

different sample runs to align DFe with conductivity (SM - Section 2). Computation of ICCF were performed with the R package `sour` freely available at the GitHub repository (Edelson et al., 2017; R Core Team, 2025). Cross-correlations between DFe and conductivity ranged between 0.51 and 0.92.

3. Results and Discussion

During the Pleistocene-Holocene transition, the ice chemistry has changed significantly. As a consequence of the sharp temperature decrease in the Northern Hemisphere during the YD, the hydrological cycle was reduced and the atmosphere became dustier, as extensively demonstrated by the higher dust, Ca^{2+} and TDFe concentration compared to the Holocene (Burgay et al., 2021a; Schüpbach et al., 2018). During the YD, dust deposited in continental Greenland was mainly sourced from the Asian (Gobi and Taklamakan) deserts (Stoll et al., 2023; Svensson et al., 2000), with limited contributions from the Saharan desert (Han et al., 2018; Nagatsuka et al., 2025; Újvári et al., 2022). Thus, the majority of dust deposited in Greenland at that time was transported across the North Pacific Ocean before reaching Greenland, indicating that EGRIP, and other Greenland ice cores, are documenting changes of dust (and iron) deposition over the HNLC North Pacific Ocean, enabling the link between Fe ice-core records with NPP sea-sediment records (Serno et al., 2015).

3.1 Fe_{ICP} record

A 17-fold increase in the median Fe_{ICP} concentration from the Early Holocene (1.76 µg L^{-1}, IQR = 3.00 µg L^{-1}) to the YD (30.16 µg L^{-1}, IQR = 30.94 µg L^{-1}) period was observed at EGRIP (Figure 1). Unfortunately, no other Fe_{ICP} record exist for Greenland ice cores, making direct comparisons with other locations impossible. Nevertheless, we can compare the Fe_{ICP} record with the NEEM TDFe record (Burgay et al., 2021a). Notwithstanding the different methodological approaches, temporal resolution of the records, and the distinct accumulation rates between the two sites (22 vs 11 cm ice equivalent per year at NEEM and EGRIP, respectively) (Schüpbach et al., 2018; Mojtabavi et al., 2019), median concentrations are of the same order of magnitude for both the Holocene (2.60 µg L^{-1}, IQR = 2.03 µg L^{-1}, at NEEM), and the YD (17.65 µg L^{-1}, IQR = 9.9 µg L^{-1}, at NEEM), suggesting overall spatially homogeneous deposition patterns and trends across the Greenland plateau on millennial time scales.

https://doi.org/10.5194/egusphere-2025-6339
Preprint. Discussion started: 27 January 2026
© Author(s) 2026. CC BY 4.0 License.

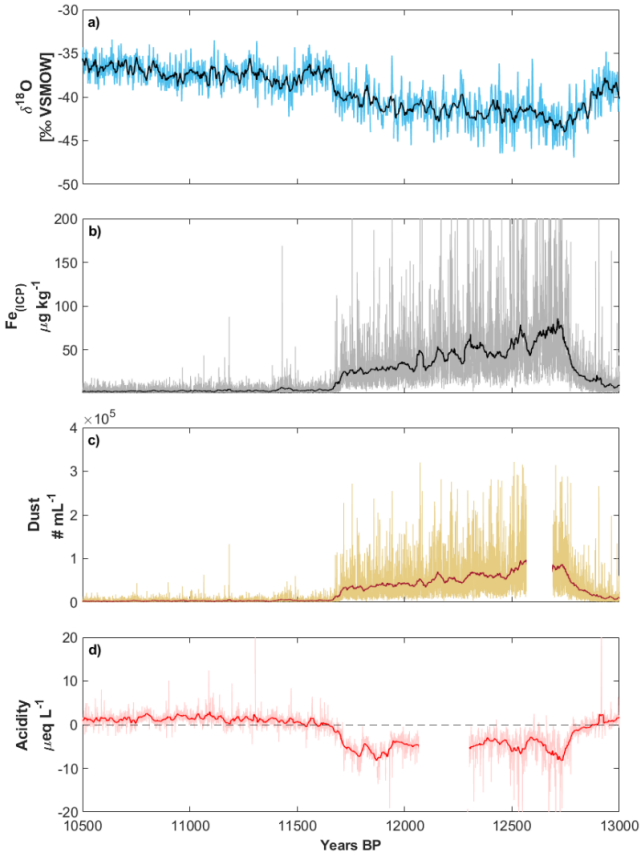

Figure 1 – Panel a): EGRIP $\delta^{18}O$ profile (Vaughn et al.). Panel b): continuous Fe_{ICP} profile. Panel c): continuous dust profile. Panel d): acidity changes. Negative µeq L^{-1} values correspond to alkaline conditions. Thick solid lines are 10-year moving averages.

Despite the relatively high Fe_{ICP} concentrations observed over Greenland during the YD, and the concurrent rise in dust fluxes inferred from sediment records in the North Pacific Ocean, NPP was at low levels. Marine sediments from the North Pacific Ocean show higher NPP during the warmer and less dusty BA and Early Holocene periods (Praetorius et al., 2015). This pattern has been linked to ocean warming, which expanded the subsurface oxygen minimum zone and promoted seafloor hypoxia. Under these low-oxygen conditions, iron is remobilized from sediments, providing a source of bioavailable Fe that further stimulated marine productivity. An additional explanation for why NPP was higher during the BA warm period in the subarctic North Pacific is associated with an increase in sea level that inundated previously exposed lands, which in turn entrained iron and other nutrients to the

https://doi.org/10.5194/egusphere-2025-6339
Preprint. Discussion started: 27 January 2026
© Author(s) 2026. CC BY 4.0 License.

marine ecosystems (Davies et al., 2011). Conversely, during the colder and dustier YD, either enhanced water stratification, which led to the consumption of major nutrients in surface waters, or a more extensive sea-ice cover, acting as a physical barrier between the atmosphere and ocean surface limiting aeolian iron deposition, played a more dominant role (Méheust et al., 2018; Kienast et al., 2004). In addition, atmospheric aerosol was more alkaline during the YD, potentially reducing Fe solubility (Delmas, 1994; Wolff et al., 1997). While these observations downscale the relevance of atmospheric Fe deposition, a continuous quantification of DFe to assess its potential availability to phytoplankton has never been performed during the Pleistocene-Holocene transition.

3.2 DFe record and implications for marine productivity

To understand whether higher Fe_{ICP} concentrations were mirrored by a similar increase in DFe during the YD compared to the Holocene, and to investigate further the effects of atmospheric iron fertilization in the HNLC North Pacific Ocean, we analyzed DFe from eight different periods (Table 1). Our continuous DFe records differ from DFe measurements commonly used in oceanographic studies (Achterberg et al., 2001) and other ice-core investigations (Winton et al., 2022; Du et al., 2019), which involve filtration with 0.2 or 0.45 µm filters followed by analysis using ICP-MS. These methods are incompatible with continuous measurements due to the filtering step. However, studies have shown that particulate iron (> 0.45 µm) can also contribute to phytoplankton growth (Kanna et al., 2020; Visser et al., 2003), suggesting that DFe as defined in this work, i.e., the leachable fraction after acidification at pH≈1.6, can be still considered as representative of the iron fraction more easily available to marine phytoplankton (Hiscock et al., 2013), although direct assessments on its true bioavailability have not yet been performed. DFe and Fe_{ICP} show a good alignment and seasonality, indicating that they share the same dust source (Figure 2). Differences in the peak shape are explained by the different methods used, with DFe showing a stronger memory effect than Fe_{ICP} due to longer mixing coils (> 2 meters). In the main text, we report only one of the eight analyzed periods for DFe as an illustrative example (Figure 2). The other periods are presented in SM-Section 3, together with the corresponding Fe_{ICP}, conductivity, acidity and DFe/Fe_{ICP} ratio records.

https://doi.org/10.5194/egusphere-2025-6339
Preprint. Discussion started: 27 January 2026
© Author(s) 2026. CC BY 4.0 License.

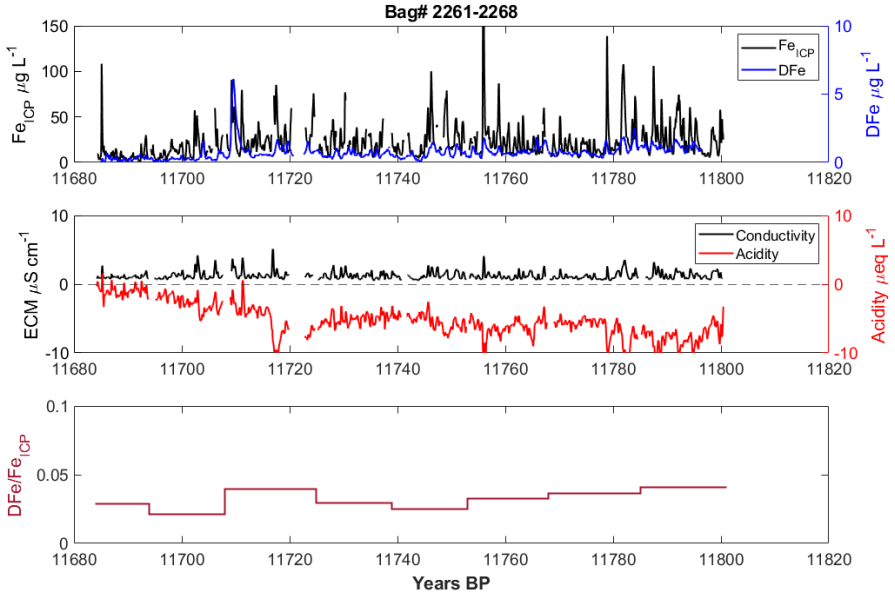

Figure 2 – Upper panel: Fe_{ICP} (black line) and DFe (blue line) during the Pleistocene-Holocene transition (11.68-11.82 ka BP). Middle panel: conductivity (ECM, black line) and acidity (red line). Bottom panel: DFe/Fe_{ICP} bag mean.

DFe median concentrations calculated over the eight investigated sections (Table 1) were at their lowest during the BA (0.35 µg L-1, IQR = 0.42 µg L^{-1}), while increasing during the YD (0.68 µg L^{-1}, IQR = 0.53 µg L^{-1}). Values during the Early Holocene were comparable to those observed during the YD (0.62 µg L^{-1}, IQR = 0.58 µg L^{-1}), contributing 20-40% to Fe_{ICP}, consistently to what was previously observed from other polar ice cores during the Holocene (Erhardt et al., 2019; Traversi et al., 2004). To compare the concentration distributions and to better investigate differences in the aeolian DFe contributions between the Early Holocene and the YD, 10 volcanic eruptions were excluded as they are known to increase DFe (Burgay et al., 2019). The volcanic events were identified based on their documented occurrence (Lin et al., 2022) and observed acidity, DFe and conductivity increases (Table S2). Then, a two-sided Wilcoxon rank sum test was applied to compare only the aeolian DFe Early Holocene and YD distributions. The test showed that the distributions during the Early Holocene and the YD (n = 7010 and, n = 14294 datapoints respectively) were significantly different (p-value < 10^{-10}), with more frequent occurrences of higher DFe concentrations in the YD (median = 0.66 µg L^{-1}) than in

https://doi.org/10.5194/egusphere-2025-6339
Preprint. Discussion started: 27 January 2026
© Author(s) 2026. CC BY 4.0 License.

the Early Holocene (median = 0.51 µg L^{-1}) (Figure S3). Although the increase in DFe median concentration between the Holocene and the YD is significant (+29%, when excluding volcanic eruptions), it is not comparable with the one observed for Fe_{ICP} (17-fold), suggesting that the stronger dust contribution during the YD was not mirrored by a similar DFe enhancement. Consequently, the DFe contribution to Fe_{ICP} decreased from an average (median) of 40% (30%) during the Holocene to an average (median) of 2% (2%) during the YD. DFe contribution slightly increased during the BA to 7% (3%).

Table 1 – Selected period (n = 8) over the Holocene, Younger Dryas (YD) and Bølling-Allerød (BA) of median DFe based on continuous sampling. Median and interquartile range (IQR) are reported. Median DFe/Fe_{ICP} ratio is calculated as a bag mean.

Period	Age /ka	Depth (top) /m	Bag #	Median (IQR) DFe /µg L^{-1}	Median (IQR) Fe_{ICP} /µg L^{-1}	Median (IQR) DFe/Fe_{ICP}
Holocene	10.32-10.39	1150.60-1154.45	2093-2100	1.03 (1.08)	1.16 (2.27)	0.43 (0.66)
Holocene	10.46-10.51	1159.95-1163.25	2110-2116	0.37 (0.35)	1.13 (2.27)	0.20 (0.14)
Holocene	10.87-10.93	1190.20-1194.05	2165-2172	0.66 (0.28)	1.54 (2.35)	0.28 (0.07)
Transition	11.68-11.80	1243.00-1246.85	2261-2268	0.61 (0.53)	16.39 (17.31)	0.03 (0.01)
YD	12.06-12.16	1256.20-1259.50	2285-2290	0.58 (0.40)	29.54 (26.73)	0.018 (0.001)
YD	12.25-12.38	1262.80-1266.65	2297-2304	0.68 (0.40)	39.07 (33.34)	0.01 (0.003)
YD	12.52-12.65	1271.60-1275.45	2313-2320	0.88 (0.74)	49.38 (44.40)	0.01 (0.004)
BA	12.90-13.07	1284.80-1293.05	2337-2352	0.35 (0.42)	7.49 (9.32)	0.03 (0.07)

These findings are compared with two other available DFe studies that applied the same methodology used in this study: one from Greenland (GRIP) (Hiscock et al., 2013), and one from Antarctica (EDC96) (Traversi et al., 2004) (Table 2). At GRIP, authors investigated DFe from a 113.4-centimeter-long section from the Holocene referring to the periods 4.51 ka (52.8 cm), 6.55 ka (24.9 cm), and 7.61 ka (35.7 cm), and from a 109.8-centimeter-long core from the Glacial (28.8 ka). They report median DFe concentrations ranging from 0.14 µg L^{-1}, during the Holocene, to 0.42 µg L^{-1}, during the Glacial. The exact values differ from the ones obtained in this study because of the limited number of ice sections analyzed and different periods investigated at GRIP. However, the orders of magnitude were comparable, although a stronger increase in DFe is observed in GRIP between the Holocene and

https://doi.org/10.5194/egusphere-2025-6339
Preprint. Discussion started: 27 January 2026
© Author(s) 2026. CC BY 4.0 License.

the Glacial (up to 3-times) than in EGRIP between the Holocene and the YD (+29%). Overall, both the GRIP and EGRIP DFe records show only a limited increase during the coldest periods with respect to the Holocene, especially when compared with the 17-fold rise in Fe_{ICP} concentrations at EGRIP between the Holocene and the YD (this study) and the 15-fold increase in TDFe at NEEM between the Holocene and the last Glacial average (Burgay et al., 2021a). Although atmospheric Fe deposition increased during the YD, the amount of Fe more easily accessible to phytoplankton was much smaller.

DFe concentration values from Greenland records contrast with the only DFe record from Antarctica. During the Antarctic Cold Reversal (ACR, 11.6-14.2 ka), DFe contributed as much as 64% of the Fe content as determined by ICP-MS (Traversi et al., 2004). In general, during cold periods (i.e., ACR and Glacial), DFe concentrations were up to 12 times (1.0 µg L^{-1}) higher than Holocene values (0.08 µg L^{-1}). Similar findings were reported from the EPICA Dome C ice core, where a tenfold increase in soluble Fe deposition fluxes during the last glacial period compared to modern values was observed (Conway et al., 2015). To explain this geographical pattern in DFe, we introduce the hypothesis that differences in aerosol acidity between Greenland and Antarctica may have played an important role.

Table 2 – Comparison between TDFe, Fe_{ICP} and DFe. Concentration (first line) and median values (second line) are reported. TDFe, Fe_{ICP} and DFe (EGRIP) are reported as 10-year averages for comparison purposes and to smooth volcanic eruption contributions. YD = Younger Dryas (12.7-12.9 ka) and BA = Bølling-Allerød (12.9-13.0 ka), ACR = Antarctic Cold Reversal (11.6-14.2 ka). n.a = not available

	NEEM[a] – TDFe /µg L^{-1}	EGRIP[b] – Fe_{ICP} /µg L^{-1}	EGRIP[c] – DFe /µg L^{-1}	GRIP[d] - DFe /µg L^{-1}	EDC96[e] – DFe /µg L^{-1}
Holocene	0.80 – 9.50	1.2 – 12.8	0.2 – 3.0	0.05-0.50	0.08-0.2
	2.30	2.70	0.60	0.14	*n.a.*
YD/ACR	6.6 – 36.2	20.8 – 78.7	0.3 – 2.6	*n.a.*	0.1-1
	17.81	42.04	0.66		*n.a.*
BA	4.9-16.1	5.9-83.4	0.1 - 2.4	*n.a.*	*n.a.*
	11.23	14.60	0.44		
Glacial	0.80 – 486.5	*n.a.*	*n.a.*	0.20-2.40	0.4-1

https://doi.org/10.5194/egusphere-2025-6339
Preprint. Discussion started: 27 January 2026
© Author(s) 2026. CC BY 4.0 License.

	17.63	0.42	*n.a.*

a) Burgay et al., 2021; b) this study; c) this study; d) Hiscock et al., 2013; e) Traversi et al., 2004.

When excluding volcanic eruptions, acidity measurements from the EGRIP ice core show median acidic values during the Early Holocene (1.06 µeq L^{-1}). During the YD, acidity decreases (Figure 1) indicating more alkaline conditions (-4.93 µeq L^{-1}) until the BA, when, however, ice pH was still slightly alkaline (-0.24 µeq L^{-1}, Figure S4). This result is consistent with previous observations showing conditions that are always-acidic in the Holocene and always-alkaline in the cold periods over Greenland due to the overwhelming contribution of carbonate dust (Delmas, 1994; Wolff et al., 1997). Considering that Fe solubility is affected by pH, even small changes in aerosol acidity can reduce Fe solubility during the YD, and therefore its availability to phytoplankton. According to theoretically calculated solubility of Fe(III), i.e., the thermodynamically stable iron form, an increase of 1 pH unit contributes to a decrease in dissolved Fe(III) up to almost 2 orders of magnitude (Conway et al., 2015), which corresponds roughly to the difference observed between Fe_{ICP} and DFe. During the BA, median DFe concentrations show values significantly lower than those observed during the Holocene (p-value $< 10^{-10}$) (Figure S3), which can also be explained by persistent alkaline conditions. In the Southern Hemisphere, the ion budget of the ice maintained more acidic conditions even during glacial periods, likely due to high biogenic SO_2 emissions, which prevented complete neutralization of the aerosol pH (Delmas, 1994; Hammer and Langway Jr, 1994). Therefore, differences in aerosol acidity between cold and warm periods in Antarctica and Greenland help understanding why DFe shows different enhancements in the two hemispheres. In Antarctica, where acidic conditions persisted both during the Holocene and Glacial periods, a higher fraction of iron remained in a dissolved, and more bioavailable form, thus supporting higher rates of phytoplankton growth and carbon sequestration mainly in the Subantarctic zone of the Southern Ocean (Martínez-García et al., 2014; Jaccard et al., 2013). On the other hand, in Greenland, stronger changes in aerosol acidity from acidic (Holocene) to alkaline (YD and BA), reduced iron solubility.

From our hemispheric comparison of DFe concentrations, we suggest a less relevant role of aeolian iron fertilization in the HNLC-North Pacific Ocean as compared to the Southern Ocean, with other

https://doi.org/10.5194/egusphere-2025-6339
Preprint. Discussion started: 27 January 2026
© Author(s) 2026. CC BY 4.0 License.

players such as water stratification, iron remobilization from sediments, and sea-ice extent having a stronger contribution in modulating NPP (Kienast et al., 2004; Praetorius et al., 2015).

3.3 Volcanic eruptions as additional sources of DFe

While the increase in DFe contained in atmospheric dust was limited during the YD compared to the Early Holocene, volcanic eruptions significantly increase iron solubility in volcanic plumes over short timescales potentially promoting transient NPP pulses in HNLC regions (Langmann et al., 2010). Iron in volcanic ash produced through magma fragmentation is essentially found in non-soluble forms, it can be mobilized through the interaction between acidic gases and particles following two main mechanisms: 1) dissolution of readily soluble iron on the surface of ash particles in the volcanic plume; 2) dissolution of silicate and non-silicate mineral components of the ash containing iron (Langmann et al., 2010). The result is the presence of high concentrations of soluble iron salts in volcanic ash such as $FeCl_x$, FeF_x (where x = 2,3) and $FeSO_4 \cdot 7H_2O$ (Langmann et al., 2010). In addition, specific magmatic conditions and high-temperature gas-ash interactions associated with CO_2-rich and SO_2-rich magmatic gases may increase the occurrence of soluble iron in the volcanic ash (Hoshyaripour et al., 2014). Together with high concentration of dissolved iron, volcanic ash also contains high concentrations of other macro- and micro-nutrients, such as PO_4^{3-}, Si, Zn, Mn, Ni, Co and Cu (Duggen et al., 2007; Kjær et al., 2013), meaning that it can sustain phytoplankton bloom and productivity over short time periods (i.e., months).

In ice cores, increases in electrical conductivity and acidity indicate the occurrence of layers corresponding to volcanic events (Hammer, 1980). Using these two markers, the average Greenland SO_4^{2-} deposition rate (Lin et al., 2022), and previous evidence of enhanced DFe concentrations and DFe/Fe_{ICP} ratio values in ice layers associated with volcanic eruptions (Burgay et al., 2019; Burgay et al., 2021b), we uniquely identified ten volcanic events across the eight EGRIP sections analyzed (Table S2, Figure S5) and we observed that the main driver of enhanced atmospheric iron solubility during the Pleistocene-Holocene transition was not increased dust transport, but rather short-term events such as volcanic eruptions. An increase in easily leachable Fe during these events may have triggered local

https://doi.org/10.5194/egusphere-2025-6339
Preprint. Discussion started: 27 January 2026
© Author(s) 2026. CC BY 4.0 License.

phytoplankton blooms in the HNLC North Pacific Ocean, in line with modern satellite observations (Olgun et al., 2011; Langmann et al., 2010). Due to the short time during which these bloom events develop, it is not possible to track them in sediment cores.

4. Conclusions

Between the Holocene and the YD, Fe_{ICP} significantly increased 17 times. However, DFe concentrations in Greenland showed only a limited enhancement during the YD compared to the Early Holocene (+29%) when excluding volcanic eruptions. These findings differ from observations in Antarctica, where DFe increased by up to 12-fold between the Holocene and the Antarctic Cold Reversal. We attribute this discrepancy to differences in atmospheric aerosol acidity between the Northern and the Southern Hemispheres, with more alkaline conditions prevailing in the former during colder, dustier periods, which reduced iron solubility in aerosols. With this work we advance an additional explanation for why aeolian iron fertilization was not the main driver in regulating NPP in the North Pacific Ocean during the YD. Nonetheless, short-term increases in DFe during volcanic eruptions may have acted as intermittent sources of bioavailable iron, potentially stimulating short-lived phytoplankton blooms. Similarly, observed increase in aerosol pH during the industrial period due to anthropogenic activities may have locally enhanced Fe availability to phytoplankton over the last decades.

Author contributions

Conceptualization: FB; **Methodology**: FB, HD, TE; **Formal analysis**: FB, HD; **Investigation**: FB, HD, TE, FS, DS, NM, FD, DZ, ASpa; **Resources**: HF, CV, CB, ASpo; **Data Curation**: FB, HD, **Writing – Original Draft**: FB, **Writing – Review & Editing:** FB, HD, TE, FS, DS, NM, FD, DZ, ASpa, HAK, HF, CV, CB, ASpo; **Visualization**: FB, **Supervision**: CV, CB, ASpo; **Project administration**: HF, CB, ASpo; **Funding acquisition**: HF, CB.

Acknowledgments

https://doi.org/10.5194/egusphere-2025-6339
Preprint. Discussion started: 27 January 2026
© Author(s) 2026. CC BY 4.0 License.

EGRIP is directed and organized by the Centre for Ice and Climate at the Niels Bohr Institute, University of Copenhagen. It is supported by funding agencies and institutions in Denmark (A. P. Møller Foundation, University of Copenhagen), USA (US National Science Foundation, Office of Polar Programs), Germany (Alfred Wegener Institute, Helmholtz Centre for Polar and Marine Research), Japan (National Institute of Polar Research and Arctic Challenge for Sustainability), Norway (University of Bergen and Trond Mohn Foundation), Switzerland (Swiss National Science Foundation), France (French Polar Institute Paul-Emile Victor, Institute for Geosciences and Environmental research), Canada (University of Manitoba) and China (Chinese Academy of Sciences and Beijing Normal University). This work has been supported by the "Programma di Ricerca in Artico" (PRA; project no. PRA2019-0011, Sentinel) and it has received funding from the European Union's Horizon 2020 research and innovation programme under grant agreement no. 689443 via project iCUPE (Integrative and Comprehensive Understanding on Polar Environments). The University of Bern acknowledges long-term financial support of the ice-core research by the Swiss National Science Foundation (grant no. 200020B_200328, 200020_172506, and 206021_170739). HAK was funded by the European H2020 Past to Future (P2F, grant 101184070) and the independent research fund Denmark (grant 1131-00007B).

https://doi.org/10.5194/egusphere-2025-6339
Preprint. Discussion started: 27 January 2026
© Author(s) 2026. CC BY 4.0 License.

REFERENCES

Achterberg, E. P., Holland, T. W., Bowie, A. R., Mantoura, R. F. C., and Worsfold, P. J.: Determination of iron in seawater, Analytica Chimica Acta, 442, 1–14, 2001.
Burgay, F., Spolaor, A., Gabrieli, J., Cozzi, G., Turetta, C., Vallelonga, P., and Barbante, C.: Atmospheric iron supply and marine productivity in the glacial North Pacific Ocean, Climate of the Past, 17, 491–505, 2021a.
Burgay, F., Erhardt, T., Lunga, D. D., Jensen, C. M., Spolaor, A., Vallelonga, P., Fischer, H., and Barbante, C.: Fe2+ in ice cores as a new potential proxy to detect past volcanic eruptions, Science of The Total Environment, 654, 1110–1117, https://doi.org/10.1016/j.scitotenv.2018.11.075, 2019.
Burgay, F., Barbaro, E., Cappelletti, D., Turetta, C., Gallet, J.-C., Isaksson, E., Stenni, B., Dreossi, G., Scoto, F., and Barbante, C.: First discrete iron (II) records from Dome C (Antarctica) and the Holtedahlfonna glacier (Svalbard), Chemosphere, 267, 129335, 2021b.
Conway, T. M., Wolff, E. W., Röthlisberger, R., Mulvaney, R., and Elderfield, H.: Constraints on soluble aerosol iron flux to the Southern Ocean at the Last Glacial Maximum, Nature communications, 6, 7850, 2015.
Davies, M., Mix, A., Stoner, J., Addison, J., Jaeger, J., Finney, B., and Wiest, J.: The deglacial transition on the southeastern Alaska Margin: Meltwater input, sea level rise, marine productivity, and sedimentary anoxia, Paleoceanography, 26, 2011.
Delmas, R. J.: Ice records of the past environment, Science of the total environment, 143, 17–30, 1994.
Du, Z., Xiao, C., Zhang, Q., Handley, M. J., Mayewski, P. A., and Li, C.: Relationship between the 2014–2015 Holuhraun eruption and the iron record in the East GRIP snow pit, Arctic, Antarctic, and Alpine Research, 51, 290–298, 2019.
Duggen, S., Croot, P., Schacht, U., and Hoffmann, L.: Subduction zone volcanic ash can fertilize the surface ocean and stimulate phytoplankton growth: Evidence from biogeochemical experiments and satellite data, Geophysical research letters, 34, 2007.
Duggen, S., Olgun, N., Croot, P., Hoffmann, L. J., Dietze, H., Delmelle, P., and Teschner, C.: The role of airborne volcanic ash for the surface ocean biogeochemical iron-cycle: a review, Biogeosciences (BG), 7, 827–844, 2010.
Edelson, R., Gelbord, J., Cackett, E., Connolly, S., Done, C., Fausnaugh, M., Gardner, E., Gehrels, N., Goad, M., and Horne, K.: Swift monitoring of NGC 4151: evidence for a second X-ray/UV reprocessing, The Astrophysical Journal, 840, 41, 2017.
Edwards, R. and Sedwick, P.: Iron in East Antarctic snow: Implications for atmospheric iron deposition and algal production in Antarctic waters, Geophysical Research Letters, 28, 3907–3910, 2001.
Edwards, R., Sedwick, P., Morgan, V., and Boutron, C.: Iron in ice cores from Law Dome: A record of atmospheric iron deposition for maritime East Antarctica during the Holocene and Last Glacial Maximum, Geochemistry, Geophysics, Geosystems, 7, 12, 2006.
Erhardt, T., Jensen, C. M., Borovinskaya, O., and Fischer, H.: Single particle characterization and total elemental concentration measurements in polar ice using continuous flow analysis-inductively coupled plasma time-of-flight mass spectrometry, Environmental science & technology, 53, 13275–13283, 2019.
Erhardt, T., Jensen, C. M., Adolphi, F., Kjær, H. A., Dallmayr, R., Twarloh, B., Behrens, M., Hirabayashi, M., Fukuda, K., and Ogata, J.: High resolution aerosol data from the top 3.8 ka of the EGRIP ice core, Earth System Science Data Discussions, 2023, 1–21, 2023.
Fischer, H., Burke, A., Rae, J., Sugden, P. J., Erhardt, T., Twarloh, B., Hörhold, M., Freitag, J., Markle, B., and Severi, M.: Limited decrease of Southern Ocean sulfur productivity across the penultimate termination, Nature Geoscience, 18, 160–166, 2025.
Francois, R., Altabet, M. A., Yu, E.-F., Sigman, D. M., Bacon, M. P., Frank, M., Bohrmann, G., Bareille, G., and Labeyrie, L. D.: Contribution of Southern Ocean surface-water stratification to low atmospheric CO 2 concentrations during the last glacial period, Nature, 389, 929–935, 1997.
Gaskell, C. M. and Sparke, L. S.: Line variations in quasars and Seyfert galaxies, Astrophysical Journal, Part 1 (ISSN 0004-637X), vol. 305, June 1, 1986, p. 175-186. Research supported by McDonald Observatory and SERC., 305, 175–186, 1986.
Gerber, T. A., Hvidberg, C. S., Rasmussen, S. O., Franke, S., Sinnl, G., Grinsted, A., Jansen, D., and Dahl-Jensen, D.: Upstream flow effects revealed in the EastGRIP ice core using Monte Carlo inversion of a two-dimensional ice-flow model, The Cryosphere, 15, 3655–3679, 2021.
Hammer, C. and Langway Jr, C.: Electrical conductivity method (ECM) stratigraphic dating of the Byrd Station ice core, Antarctica, Annals of Glaciology, 20, 115–120, 1994.
Hammer, C. U.: Acidity of polar ice cores in relation to absolute dating, past volcanism, and radio–echoes, Journal of Glaciology, 25, 359–372, 1980.

https://doi.org/10.5194/egusphere-2025-6339
Preprint. Discussion started: 27 January 2026
© Author(s) 2026. CC BY 4.0 License.

Han, C., Do Hur, S., Han, Y., Lee, K., Hong, S., Erhardt, T., Fischer, H., Svensson, A. M., Steffensen, J. P., and Vallelonga, P.: High-resolution isotopic evidence for a potential Saharan provenance of Greenland glacial dust, Scientific reports, 8, 1–9, 2018.
Hiscock, W. T., Fischer, H., Bigler, M., Gfeller, G., Leuenberger, D., and Mini, O.: Continuous flow analysis of labile iron in ice-cores, Environmental science & technology, 47, 4416–4425, 2013.
Hoshyaripour, G., Hort, M., Langmann, B., and Delmelle, P.: Volcanic controls on ash iron solubility: New insights from high-temperature gas–ash interaction modeling, Journal of volcanology and geothermal research, 286, 67–77, 2014.
Hvidberg, C. S., Grinsted, A., Dahl-Jensen, D., Khan, S. A., Kusk, A., Andersen, J. K., Neckel, N., Solgaard, A., Karlsson, N. B., and Kjær, H. A.: Surface velocity of the Northeast Greenland Ice Stream (NEGIS): assessment of interior velocities derived from satellite data by GPS, The Cryosphere, 14, 3487–3502, 2020.
Jaccard, S. L., Hayes, C. T., Martinez-Garcia, A., Hodell, D. A., Anderson, R. F., Sigman, D. M., and Haug, G.: Two modes of change in Southern Ocean productivity over the past million years, Science, 339, 1419–1423, 2013.
Kanna, N., Lannuzel, D., van der Merwe, P., and Nishioka, J.: Size fractionation and bioavailability of iron released from melting sea ice in a subpolar marginal sea, Marine chemistry, 221, 103774, 2020.
Kaufmann, P. R., Federer, U., Hutterli, M. A., Bigler, M., Schüpbach, S., Ruth, U., Schmitt, J., and Stocker, T. F.: An improved continuous flow analysis system for high-resolution field measurements on ice cores, Environmental science & technology, 42, 8044–8050, 2008.
Kienast, S. S., Hendy, I. L., Crusius, J., Pedersen, T. F., and Calvert, S. E.: Export production in the subarctic North Pacific over the last 800 kyrs: No evidence for iron fertilization?, Journal of Oceanography, 60, 189–203, 2004.
Kjær, H. A., Vallelonga, P., Svensson, A., Kristensen, M. E. L., Tibuleac, C., and Bigler, M.: Continuous flow analysis method for determination of dissolved reactive phosphorus in ice cores, Environmental science & technology, 47, 12325–12332, 2013.
Kjær, H. A., Vallelonga, P., Svensson, A., Elleskov L. Kristensen, M., Tibuleac, C., Winstrup, M., and Kipfstuhl, S.: An optical dye method for continuous determination of acidity in ice cores, Environmental science & technology, 50, 10485–10493, 2016.
Lambert, F., Tagliabue, A., Shaffer, G., Lamy, F., Winckler, G., Farias, L., Gallardo, L., and De Pol-Holz, R.: Dust fluxes and iron fertilization in Holocene and Last Glacial Maximum climates, Geophysical Research Letters, 42, 6014–6023, 2015.
Lambert, F., Opazo, N., Ridgwell, A., Winckler, G., Lamy, F., Shaffer, G., Kohfeld, K., Ohgaito, R., Albani, S., and Abe-Ouchi, A.: Regional patterns and temporal evolution of ocean iron fertilization and CO2 drawdown during the last glacial termination, Earth and Planetary Science Letters, 554, 116675, 2021.
Langmann, B., Zakšek, K., Hort, M., and Duggen, S.: Volcanic ash as fertiliser for the surface ocean, Atmos. Chem. Phys., 10, 3891–3899, 10.5194/acp-10-3891-2010, 2010.
Lin, J., Svensson, A., Hvidberg, C. S., Lohmann, J., Kristiansen, S., Dahl-Jensen, D., Steffensen, J. P., Rasmussen, S. O., Cook, E., and Kjær, H. A.: Magnitude, frequency and climate forcing of global volcanism during the last glacial period as seen in Greenland and Antarctic ice cores (60–9 ka), Climate of the Past, 18, 485–506, 2022.
Lohan, M. C., Aguilar-Islas, A. M., and Bruland, K. W.: Direct determination of iron in acidified (pH 1.7) seawater samples by flow injection analysis with catalytic spectrophotometric detection: Application and intercomparison, Limnology and Oceanography: Methods, 4, 164–171, 2006.
Martin, J., Gordon, M., and Fitzwater, S.: Iron in Antarctic waters, Nature, 345, 156–158, 10.1038/345156a0, 1990.
Martin, J. H. and Fitzwater, S. E.: Iron deficiency limits phytoplankton growth in the north-east Pacific subarctic, Nature, 331, 341–343, 1988.
Martínez-García, A., Sigman, D. M., Ren, H., Anderson, R. F., Straub, M., Hodell, D. A., Jaccard, S. L., Eglinton, T. I., and Haug, G. H.: Iron fertilization of the Subantarctic Ocean during the last ice age, Science, 343, 1347–1350, 2014.
Méheust, M., Stein, R., Fahl, K., and Gersonde, R.: Sea-ice variability in the subarctic North Pacific and adjacent Bering Sea during the past 25 ka: new insights from IP 25 and U k′ 37 proxy records, arktos, 4, 8, 2018.
Mills, M. M., Ridame, C., Davey, M., La Roche, J., and Geider, R. J.: Iron and phosphorus co-limit nitrogen fixation in the eastern tropical North Atlantic, Nature, 429, 292–294, 2004.
Mojtabavi, S., Wilhelms, F., Cook, E., Davies, S., Sinnl, G., Skov Jensen, M., Dahl-Jensen, D., Svensson, A., Vinther, B., and Kipfstuhl, S.: A first chronology for the East Greenland Ice-core Project (EGRIP) over the Holocene and last glacial termination, 2019.
Nagatsuka, N., Goto-Azuma, K., Nagashima, K., Fujita, K., Komuro, Y., Hirabayashi, M., Ogata, J., Fukuda, K., Ogawa-Tsukagawa, Y., and Kitamura, K.: A 100-Year record of mineralogical variations in Northeastern Greenland ice-core dust: Insights from individual particle analysis, EGUsphere, 2025, 1–39, 2025.

https://doi.org/10.5194/egusphere-2025-6339
Preprint. Discussion started: 27 January 2026
© Author(s) 2026. CC BY 4.0 License.

Olgun, N., Duggen, S., Croot, P. L., Delmelle, P., Dietze, H., Schacht, U., Oskarsson, N., Siebe, C., Auer, A., and Garbe-Schönberg, D.: Surface ocean iron fertilization: the role of subduction zone and hotspot volcanic ash and fluxes into the Pacific Ocean, Global Biogeochemical Cycles, 25, GB4001, 2011.
Praetorius, S. K., Mix, A. C., Walczak, M., Wolhowe, M. D., Addison, J. A., and Prahl, F. G.: North Pacific deglacial hypoxic events linked to abrupt ocean warming, Nature, 527, 362–366, 2015.
R: A language and environment for statistical computing: https://www.R-project.org/, last
Schüpbach, S., Fischer, H., Bigler, M., Erhardt, T., Gfeller, G., Leuenberger, D., Mini, O., Mulvaney, R., Abram, N. J., and Fleet, L.: Greenland records of aerosol source and atmospheric lifetime changes from the Eemian to the Holocene, Nature communications, 9, 1–10, 2018.
Serno, S., Winckler, G., Anderson, R. F., Maier, E., Ren, H., Gersonde, R., and Haug, G. H.: Comparing dust flux records from the Subarctic North Pacific and Greenland: Implications for atmospheric transport to Greenland and for the application of dust as a chronostratigraphic tool, Paleoceanography, 30, 583–600, 2015.
Simonsen, M. F., Cremonesi, L., Baccolo, G., Bosch, S., Delmonte, B., Erhardt, T., Kjær, H. A., Potenza, M., Svensson, A., and Vallelonga, P.: Particle shape accounts for instrumental discrepancy in ice core dust size distributions, Climate of the Past, 14, 601–608, 2018.
Stoll, H.: 30 years of the iron hypothesis of ice ages, 2020.
Stoll, N., Westhoff, J., Bohleber, P., Svensson, A., Dahl-Jensen, D., Barbante, C., and Weikusat, I.: Chemical and visual characterisation of EGRIP glacial ice and cloudy bands within, The Cryosphere, 17, 2021–2043, 2023.
Svensson, A., Biscaye, P. E., and Grousset, F. E.: Characterization of late glacial continental dust in the Greenland Ice Core Project ice core, Journal of Geophysical Research: Atmospheres, 105, 4637–4656, 2000.
Traversi, R., Barbante, C., Gaspari, V., Fattori, I., Largiuni, O., Magaldi, L., and Udisti, R.: Aluminium and iron record for the last 28 kyr derived from the Antarctic EDC96 ice core using new CFA methods, Annals of Glaciology, 39, 300–306, 2004.
Újvári, G., Klötzli, U., Stevens, T., Svensson, A., Ludwig, P., Vennemann, T., Gier, S., Horschinegg, M., Palcsu, L., and Hippler, D.: Greenland ice core record of last glacial dust sources and atmospheric circulation, Journal of Geophysical Research: Atmospheres, 127, e2022JD036597, 2022.
Vallelonga, P., Barbante, C., Cozzi, G., Gabrieli, J., Schüpbach, S., Spolaor, A., and Turetta, C.: Iron fluxes to Talos Dome, Antarctica, over the past 200 kyr, Climate of the Past, 9, 597–604, 2013.
Vaughn, B., Morris, V., ANunn, R., AJones, T., ABrashear, C., ARozmiarek, K., AHughes, A., ASkorski, W., ABorn, A., ABuizert, C., ADahl-Jensen, D., AGkinis, V., AHolme, C., AJohnsen, S., AJensen, M., AKjellman, S., ALangebroek, P., AMekhaldi, F., ANisancioglu, K., AQuistgaard, T., ARheinlænder, J., ARasmussen, S., ASimon, M., ASinnl, G., ASowers, T., ASteen-Larsen, H., ASteffensen, J., ASkorski, W., AVinther, B., AWong, J., AWhite, J., and Center, D. A. D.: EGRIP water isotope data 21.5 m (meters) to 2120.7 m depth at 5 cm resolution, from continuous flow analysis (CFA) [dataset],
Visser, F., Gerringa, L., Van der Gaast, S., De Baar, H., and Timmermans, K.: The role of the reactivity and content of iron of aerosol dust on growth rates of two Antarctic diatom species 1, Journal of Phycology, 39, 1085–1094, 2003.
Winton, V., Bowie, A., Curran, M., and Moy, A.: Enhanced deposition of atmospheric soluble iron by intrusions of marine air masses to East Antarctica, Journal of Geophysical Research: Atmospheres, 127, e2022JD036586, 2022.
Wolff, E. W., Moore, J. C., Clausen, H. B., and Hammer, C. U.: Climatic implications of background acidity and other chemistry derived from electrical studies of the Greenland Ice Core Project ice core, Journal of Geophysical Research: Oceans, 102, 26325–26332, 1997.
Yoshida, T., Hayashi, K.-i., and Ohmoto, H.: Dissolution of iron hydroxides by marine bacterial siderophore, Chemical geology, 184, 1–9, 2002.